Observation of single phonon-mediated quantum transport in a silicon single-electron CMOS transistor by RMS noise analysis

Stefano Bigoni,[1] Marco L. V. Tagliaferri,[1, 2] Dario Tamascelli,[3] Sebastiano Strangio,[4] Roberto Bez,[4] Paolo Organtini,[4] Giorgio Ferrari,[5] and Enrico Prati[1, a)]

[1)]*Istituto di Fotonica e Nanotecnologie, Piazza Leonardo da Vinci 32, 20133 Milan, Italy*
[2)]*Université Grenoble Alpes, CEA, IRIG-Pheliqs, 38000 Grenoble, France*
[3)]*Università degli Studi di Milano, Dip. di Fisica "Aldo Pontremoli", Via Celoria 16, I-20133 Milano, Italy*
[4)]*LFoundry, Via A. Pacinotti 7, 67051 Avezzano, L'Aquila, Italy*
[5)]*Politecnico di Milano, Piazza Leonardo da Vinci 32, 20133 Milan, Italy*

(Dated: July 14, 2020)

We explore phonon-mediated quantum transport through electronic noise characterization of a commercial CMOS transistor. The device behaves as a single electron transistor thanks to a single impurity atom in the channel. A low noise cryogenic CMOS transimpedance amplifier is exploited to perform low-frequency noise characterization down to the single electron, single donor and single phonon regime simultaneously, not otherwise visible through standard stability diagrams. Single electron tunneling as well as phonon-mediated features emerges in rms-noise measurements. Phonons are emitted at high frequency by generation-recombination phenomena by the impurity atom. The phonon decay is correlated to a Lorentzian $1/f^2$ noise at low frequency.

Single-phonon mediated quantum transport is observed through electronic noise characterization in a single electron quantum dot induced in an industrial silicon transistor operated at cryogenic temperature. Phonon-mediated quantum transport has been reported as a byproduct of Coulomb blockade electronic spectroscopy of semiconductor quantum dots at cryogenic temperatures[1–6]. On the other hand, the need of spectroscopy methods for the characterization of quantum dots in the few-electron (or hole) regime has led to reflectometry[7] which probes charge tunneling transitions through the dispersive shift of a resonator connected to a gate electrode.

We have already demonstrated the control of industrial and pre-industrial silicon nanotransistors at cryogenic temperatures, down to the single electron[8] and single atom regime[9,10], respectively. We developed custom cryogenic CMOS amplifiers[11] to study single charge dynamics and reported performances[12] compatible with the readout of spin qubits in silicon[13]. Here we explore the microscopic nature of phonon-mediated quantum transport through the current of an industrial CMOS silicon transistor at 4.2 K using a cryogenic CMOS transimpedance amplifier. In the past, noise characteristics in nanowires have already been explored[14], revealing insights on the microscopic nature of the processes, including generation-recombination phenomena. Here, we base our study on the characterization of the electronic noise instead of current as usual. We exploit it to magnify the single atom regime, where few phonons processes occur. Indeed, because of their relatively small magnitude, phonon-mediated quantum transport becomes visible only by Root Mean Square (RMS) noise measurements.

By exploiting a cryogenic CMOS transimpedance amplifier, we identify additional quantum transport features generated by few phonon-emission at the single impurity site and we observe a low frequency noise spectral density behaving as $1/f^2$. More in general, we show that noise measurements provide complementary knowledge with respect of standard DC current characterization, thanks to the information provided by both the RMS and the spectrum of the noise of the current.

The single-gated silicon n-type MOSFET is produced by LFoundry by a standard 110 nm CMOS lithography process, with a nominal supply voltage of 1.2 V. Although several different samples with different form factors $W \times L$ have been characterized, for the sake of consistency we report the characterization of the most representative one, of nominal width $W = 140$ nm and length $L = 100$ nm. The source electrode is kept at zero potential and, in the following, potentials applied to the other terminals are referred to it. In this kind of devices, below 10 K, disorder at the Si/SiO$_2$ interface[15,16] dominates electron confinement, as along as the effect of a gate voltage V_g near threshold gives rise to local electrostatic potential minima through which electron tunneling can occur. As a consequence, the formation of one or more quantum dots in the channel of the transistor arises. In addition, in short channel devices (below 100-200 nm) donor atoms (here As) can be randomly diffused from the source or drain contacts in the channel region, sufficiently far to lie approximately in the center of the channel and thus contributing to additional quantum transport channels[9].

Measurements were carried out at 4.2 K, by dipping the samples in liquid ^{4}He, in order to observe electron localization and quantum transport in the device. We used a custom-made steel dip-stick provided of a 16-pin dual-in-line carrier and a custom cryogenic amplifier[12,15], described below, as a pre-amplification stage. Such cryogenic amplifier allowed to obtain simultaneous measurements of source-drain DC current I_{ds} and its rms noise level I_{RMS}, or alternatively, coupled to a custom spectrum analyzer[17], the noise power spectral density S_I at constant applied voltages (Figure 1a). Other relevant quantities like the differential conductance $g_{ds,\text{diff}} =$
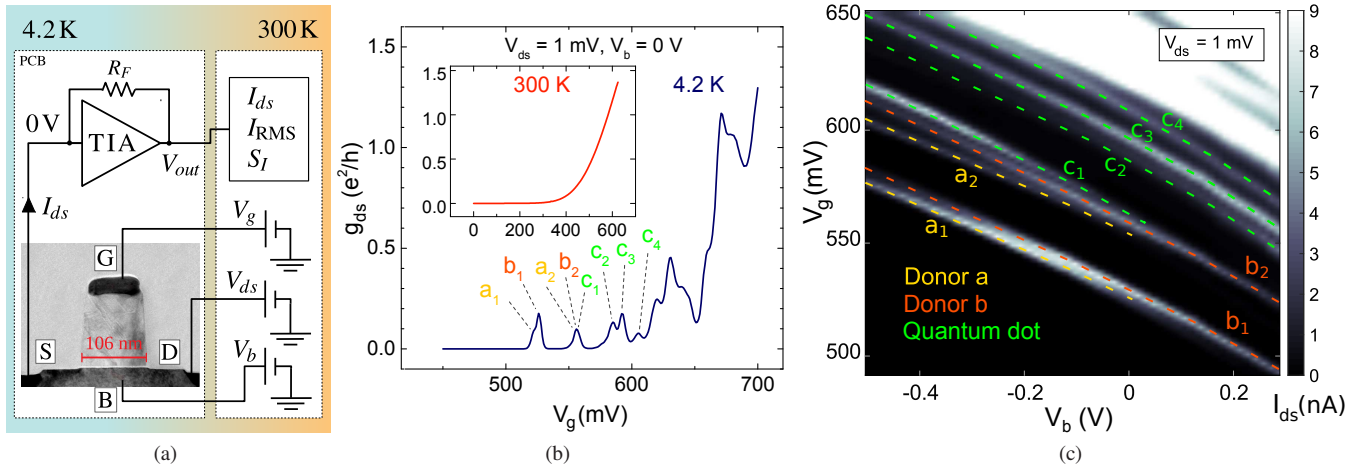
Figure 1. (a) TEM image of a device nominally identical to the device under test, with basic schematic of the measurement setup. The main element of the measurement circuit consists of the cryogenic transimpedance amplifier (TIA) operating at the same temperature of the device. In red, it is reported the actual channel length of 106 nm. (b) Device transconductance ($g_{ds} = I_{ds}/V_g$) at both 4.2 K and room temperature, respectively: Coulomb blockade (CB) peaks are visible at 4.2 K, in contrast to the standard n-type MOSFET behavior at room temperature. The peaks associated to the donor states exhibit high conductance in terms of e^2/h indicating a strong coupling regime. CB peaks are labeled as in the $V_g - V_b$ stability diagram. (c) Source-drain current I_{ds} versus both the gate and the bulk voltage. The bulk electrode is operated as a back-gate: the CB peaks at different bulk voltage form parallel lines which give information about the localized states. Different slopes are associated to distinct islands: more specifically the red (b_1, b_2) and the yellow (a_1, a_2) dashed lines correspond to two donors, while the green ones (c_1 to c_4) are associated to a disorder related electrostatically defined quantum dot.

$\delta I_{ds}/\delta V_{ds}$ and transconductance $g_{m,\text{diff}} = \delta I_{ds}/\delta V_g$ are calculated from the DC measurements.

The key element of our measurement setup is a custom CMOS amplifier designed to operate at 4.2 K, which reduces the thermal noise of the resistors and transistors. In addition, the length of the connections between the cryogenic device and the first amplification stage is reduced from meters of a standard room temperature solution to the scale of the centimeter, thus cutting most of the parasitic capacitance and correspondingly the high frequency noise on current measurements, with respect to room-temperature amplification. The amplifier uses a transimpedance architecture with a resistive feedback that sets the current-to-voltage conversion factor. The feedback resistor R_F is chosen as a trade-off between the input-referred current noise and the signal bandwidth, both inversely proportional to the resistor value. For better consistency, all the measurements reported in this work are taken with a feedback resistor of $200\,\text{M}\Omega$ at 4.2 K that provides a bandwidth of 2.8 kHz and a noise level below to $10\,\text{fA}/\sqrt{\text{Hz}}$. The cryogenic amplifier has been implemented in a standard $0.35\,\mu\text{m}$ CMOS technology previously characterized at $4.2\,\text{K}^{11}$, it occupies $0.3\,\text{mm}^2$ and has a static current consumption of $600\,\mu\text{A}$ with a power supply of 3.3 V.

Conductance peaks in Fig. 1b show the resonant tunneling and Coulomb blockade behaviour in the device. The bulk potential V_b is used as a back-gate to tune the electrostatic coupling between the localized states in the channel and the source/drain contacts, which behave as reservoirs with continuous energy spectrum up to their chemical potential[18–21]. The V_g vs V_b stability diagram at a constant bias of $V_{ds} = 1\text{mV}$ is reported in Fig. 1c. As distinct confinement centers are coupled to the bulk gate differently depending on their position,

the resonant tunneling levels result grouped as parallel lines of different slope associated to distinct electrostatic quantum dots and donors centred in the channel. The 2D stability diagrams in Fig. 2 of current, differential conductance and differential transconductance versus V_{ds} and V_g give a broader view of the spectroscopy of the states in the device and are complemented by an rms stability diagram.

The association of the first electron levels of the device to two group V donor atoms is justified by three experimental facts. First, it is the presence of the two pairs of parallel lines (a_1, a_2 and b_1, b_2 respectively) in Fig. 1c with similar charging energy, with no further states at higher energy. It corresponds to the fact that a group V donor can bound only two electrons, forming a neutral (D^0) and a negatively charged (D^-) states[20]. Second, the charging energy of both is about 19 meV which is in the range of around 15-20 meV reported in several works[19,22,23], Finally, conduction band transport occurs starting from 40-50 meV above such energy levels, which corresponds to the $\approx 45\text{meV}$ ionization energy of the ground state referred to the conduction band, which falls around 610 mV at 4.2K as from Fig. 1b. We thus reasonably conclude that, as expected by the fact that the channel is only 100 nm long and the annealing process operated during the fabrication, there are two donors participating to the transport in the channel, both by D^0 and D^- states. The values of the charging and ionization energies along with the arsenic implantation for the ohmic contacts definition, suggest the single donors to be As atoms. At higher energy with respect to the donor states, the family of peaks referred to as c have a different slope and energy spacing than the donors, allowing occupation greater than two, which we attribute to a quantum dot electrostatically defined by some interface disorder which is not screened at cryogenic
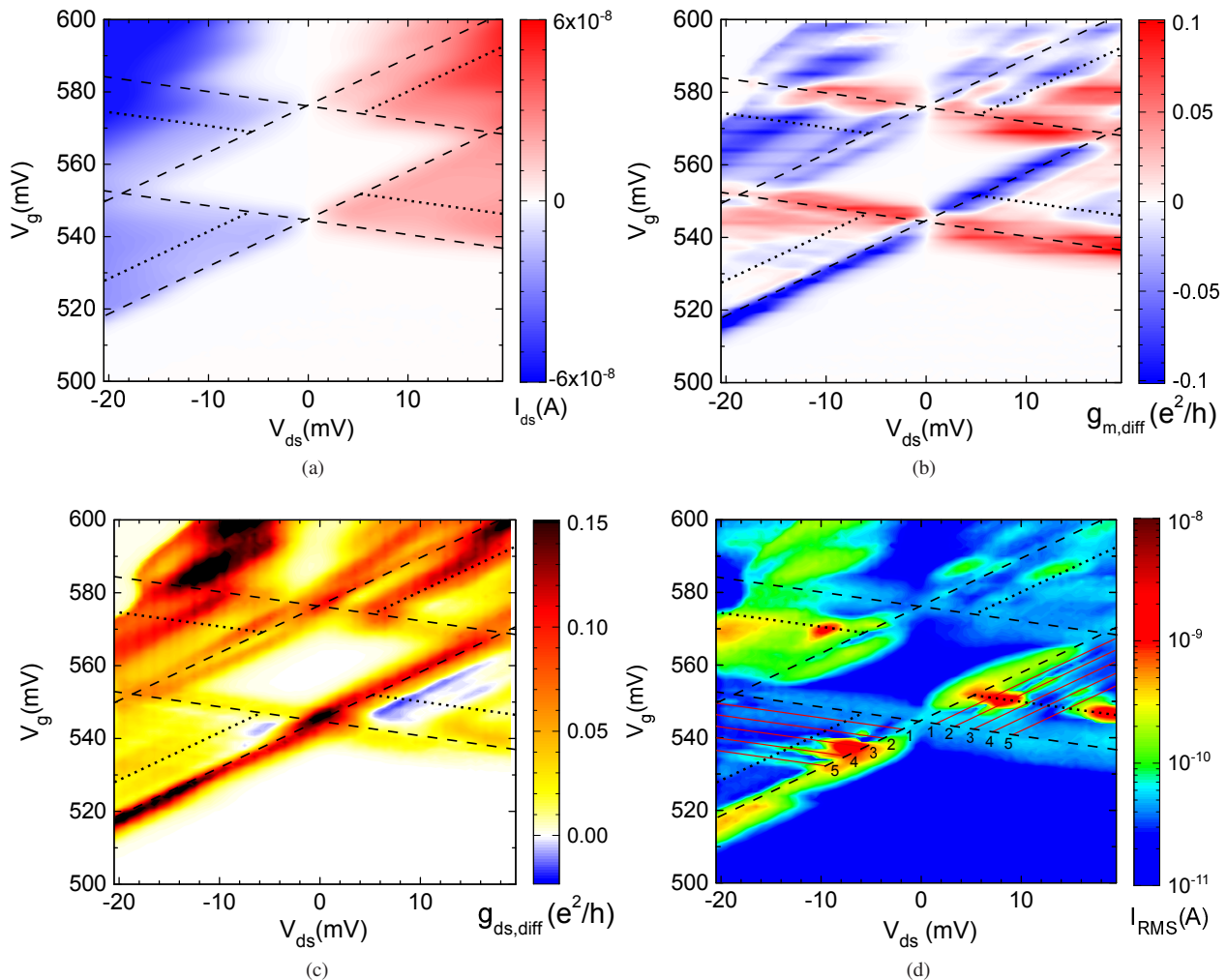
Figure 2. Stability diagrams of the first Coulomb diamond at $V_b = 0\,\text{V}$ and $T = 4.2\,\text{K}$: (a) source-drain current, (b) gate differential transconductance (c) drain differential conductance (d) current RMS noise in logarithmic scale, versus gate and drain voltage. Measured points are interpolated along contour lines for better visualization, the actual resolution being $\delta V_{ds} = 0.5\,\text{mV}$ and $\delta V_g = 1\,\text{mV}$. The same set of lines is drawn in all four diagrams: black dashed lines highlight the lowest Coulomb diamond, corresponding to the first localized state allowing transport in the device; dotted lines are associated to an excited state about 5 meV above the ground state. The lines marked in red (d) highlight parallel features associated to phonon-mediated transport, their energy separation being approximately around 2.3 meV. The corresponding left and right lines are aligned to the V_g axis. Although they are not all equally visible, the lines highlight the regular spacing.

temperature and ultra-diluted electron density. Such observations are confirmed by the rigid translation of the stability diagram fingerprint given by the first and the second peaks in Fig. 2 that we observed by changing the bulk voltage. An interesting peculiarity of this device consists of its high conductance in units of $e^2/\hbar$ which suggests a strong coupling regime of the donor states with the contacts.

We now turn to the investigation of the electron transport in the device as carried out by first analyzing the Coulomb blockade diamond structures that best fit the data plotted in Fig. 2 according to the constant interaction model[24]. Such measurements were all taken during the same thermal cycle, different than those of Fig. 1c: a small shift of the resonant tunneling features is observed between different thermal cycles, generally attributed to a different configuration of frozen

surrounding charges in distant interface defects, but the relative positions of the peaks and the geometry of the Coulomb diamonds remains the same. Figure 2d) shows the RMS of the drain current as a function of the gate and drain voltages. For each measurement point the acquisition time was of 0.1 s enabling the calculation of the RMS value of the current noise on the full bandwidth of the amplifier starting from 10 Hz. The use of the cryogenic amplifier enhanced the RMS stability diagram measurements, as more resonant tunneling features were observed than in similar diagrams obtained with room-temperature amplification (see Supplementary Material). Closely spaced equidistant parallel lines terminating on the lines of the first electron state are detected (red lines in Fig. 2d): such features can not be attributed neither to density-of-state fluctuations in the contacts nor to excited

states of the donor because they are symmetric and cross in points of zero bias towards lowest gate voltages respectively. Interestingly, their identical periodic spacing for both positive and negative V_{ds} bias voltage points towards tunneling events assisted by phonon emission on the two sides, as from Ref. 2. Such transport regime is further investigated in the following by looking at the noise spectrum.

The width and height of the main Coulomb diamond in Fig. 2, along with the slopes of its edges and of the red lines in Fig. 1c, are used to extract information about the donor states and the coupling with the transistor electrodes. From the width (i.e. the voltage distance of the corners with respect to the zero bias vertical line) the charging energy is estimated as $E_{ch} = (19 \pm 1)\,\text{meV}$.

The lever-arm factor is estimated to be $\alpha = 0.59 \pm 0.05$. This value allows to calculate the total capacitance C and the other values as follows:

C	C_g	C_s	C_d	C_b
13 aF	7.6 aF	2.3 aF	2.5 aF	0.4 aF

Despite the uncertainty in these values due to graphical extrapolation, comparison between them provides insight on the location of the donor atom(s): since $C_s \simeq C_d$, the donor is similarly coupled to the source and drain contacts and therefore located near the center of the channel, as most probable from theory in order to observe some current flow.

The phonon energy spacing Δ_{ph}, again converted from the spacing between the corresponding red lines using the same lever-arm factor is around 2.3 meV. Assuming the phonon velocity in silicon of about $v = 7 \times 10^5\,\text{cm/s}$, the estimation of the corresponding wavelength λ is of the order of 11 nm. In the hypothesis of an open phonon cavity originating these electron transport resonances, as from Ref. 3, the length L of such a cavity corresponds to $\lambda/4$; the resulting length of 2.6 nm is compatible with the longitudinal Bohr orbit diameter of As atoms in silicon which is 2.36 nm[20,25].

Additional information on the phonon-mediated tunneling process has been obtained by measuring the power spectral density of the source-drain current noise. For these measurements the device was tuned to a constant bias $V_{ds} = 14$ mV and to different values of V_g in a range where the evenly-spaced lines associated to phonon-mediated tunneling occurs. Fig. 3(a) shows the comparison of the noise spectrum in regions where: current regularly flows through a state at energy far from the transition to the blocked regime, which results as typical $1/f$ noise (black dot), at the edge of the stability diagram where $1/f$ noise is observed at low frequency (gray), and in the regions where phonon emission occurs (yellow, orange, red, purple and pink dots). In this latter case a $1/f^2$ trend is observed according whether the respective lines are visible in the RMS stability diagrams at that bias voltage V_{DS}. Such low frequency noise can not be associated to the Lorentzian noise of a single defect as the characteristic frequency of the Lorentzian curve fitting the spectra is constant (around 12 Hz) in the whole V_g range of the parallel features, differently than a charge Random Telegraph Signal (RTS). Furthermore, at such low temperature RTS of a single defect arises in energy intervals of few meV only. The
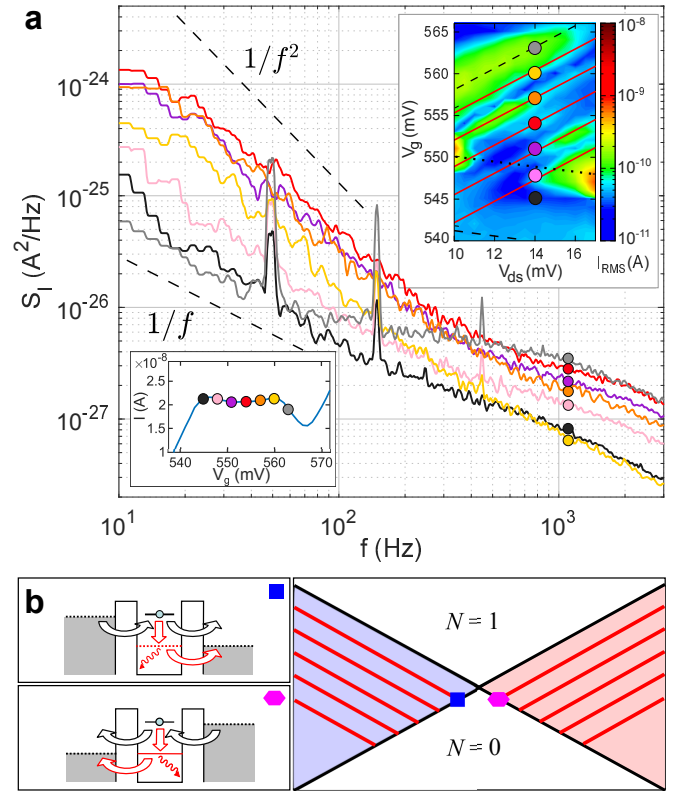

Figure 3. (a) Selected noise spectra at $V_{ds} = 14$ mV, in a region of the stability diagram where evenly spaced phononic lines are observed (see Fig. 2d). The upper inset zooms the I_{RMS} data in that portion, measured over the full bandwidth of the acquisition system. The dots indicate the different V_g values at which each respective noise spectrum was measured. The colored ones correspond to enhanced-current lines at 549, 551, 554, 557 and 560 mV while the black and grey ones, at 543 and 563 mV respectively, where the current flows but the phonons are not involved, are shown for comparison. The dashed lines are guides to the eye of the relevant slopes. The peaks observed in the black and grey spectra at 50, 150 and 450 Hz are due to supply current noise. The lower inset shows the current at $V_d = 14$ mV indicating the location of the considered working points in a transport region between Coulomb diamonds. (b) Sketch of the phonon-mediated transport in correspondence of the first phonon-line. On the left, the mechanism for the negative (blue square) and positive (violet hexagon) current, respectively. On the right, the reference point in the current stability diagram. The red lines indicate where higher RMS noise emerges, not visible by the sole current.

spectra of Figure 3a corresponding to phonon lines are fitted by $1/f$ noise with two Lorentzian noise phenomena at 12 Hz and 2800 Hz respectively, both irrespective from the gate voltage. As they are observed only in correspondence of visible phonon emission lines, we attribute them to the decay of high frequency phonons to low frequency acoustic phonons during the cooling process of the crystal[26–29]. The Fig. 3(b) shows the microscopic mechanism of phonon emission for the negative and positive current respectively. To summarize, the single phonon-mediated regime of the quantum transport occurs in such single electron filling of the single donor channel regime.

To conclude, we observe single phonon-mediated quantum

transport by tracking the RMS noise in a nano-transistor operated in the single atom and single electron regime. The use of a cryogenic amplifier makes such measurement effective, by reducing the instrumental noise and the electromagnetic noise affecting the measurements when the amplification system is far from the device under test. The characterization of a commercial single electron transistor revealed the presence of a dopant in the channel, likely originated by unintentional diffusion from the source/drain contacts. The RMS measurements indicate the presence of few- down to single-phonon mediated tunneling, for which the low frequency spectrum results a Lorentzian typical of generation-recombination processes.

Data are available upon reasonable request.

REFERENCES

[1] T. Fujisawa, T. H. Oosterkamp, W. G. Van der Wiel, B. W. Broer, R. Aguado, S. Tarucha, and L. P. Kouwenhoven, Science **282**, 932 (1998).

[2] F. A. Zwanenburg, C. E. van Rijmenam, Y. Fang, C. M. Lieber, and L. P. Kouwenhoven, Nano letters **9**, 1071 (2009).

[3] C. C. Escott, F. A. Zwanenburg, and A. Morello, Nanotechnology **21**, 274018 (2010).

[4] G. Granger, D. Taubert, C. Young, L. Gaudreau, A. Kam, S. Studenikin, P. Zawadzki, D. Harbusch, D. Schuh, W. Wegscheider, et al., Nature Physics **8**, 522 (2012).

[5] F. R. Braakman, P. Barthelemy, C. Reichl, W. Wegscheider, and L. M. Vandersypen, Applied Physics Letters **102**, 112110 (2013).

[6] S. Braig and K. Flensberg, Physical Review B **68**, 205324 (2003).

[7] A. Crippa, R. Ezzouch, A. Aprá, A. Amisse, R. Laviéville, L. Hutin, B. Bertrand, M. Vinet, M. Urdampilleta, T. Meunier, et al., Nature communications **10**, 1 (2019).

[8] M. Turchetti, H. Homulle, F. Sebastiano, G. Ferrari, E. Charbon, and E. Prati, Applied Physics Express **9**, 014001 (2015).

[9] G. Leti, E. Prati, M. Belli, G. Petretto, M. Fanciulli, M. Vinet, R. Wacquez, and M. Sanquer, Applied Physics Letters **99**, 242102 (2011).

[10] A. Crippa, M. L. Tagliaferri, D. Rotta, M. De Michielis, G. Mazzeo, M. Fanciulli, R. Wacquez, M. Vinet, and E. Prati, Physical Review B **92**, 35424 (2015).

[11] F. Guagliardo and G. Ferrari, in *Low-noise current measurements on quantum devices opera*, edited by E. Prati and T. Shinada (Pan Stanford Publishing, 2013) pp. 187–210.

[12] M. L. V. Tagliaferri, A. Crippa, S. Cocco, M. De Michielis, M. Fanciulli, G. Ferrari, and E. Prati, IEEE Transactions on Instrumentation and Measurement **65**, 1827 (2016).

[13] E. Prati and A. Morello, Single-Atom Nanoelectronics , 5 (2013).

[14] S. Vitusevich and I. Zadorozhnyi, Semiconductor Science and Technology **32**, 043002 (2017).

[15] G. Mazzeo, E. Prati, M. Belli, G. Leti, S. Cocco, M. Fanciulli, F. Guagliardo, and G. Ferrari, Applied Physics Letters **100**, 213107 (2012).

[16] M. L. V. Tagliaferri, A. Crippa, M. De Michielis, G. Mazzeo, M. Fanciulli, and E. Prati, Physics Letters A **380**, 1205 (2016).

[17] M. Sampietro, L. Fasoli, and G. Ferrari, Review of scientific instruments **70**, 2520 (1999).

[18] G. Lansbergen, R. Rahman, C. Wellard, I. Woo, J. Caro, N. Collaert, S. Biesemans, G. Klimeck, L. Hollenberg, and S. Rogge, Nature Physics **4**, 656 (2008).

[19] E. Prati, M. Belli, S. Cocco, G. Petretto, and M. Fanciulli, Applied physics letters **98**, 053109 (2011).

[20] E. Prati and T. Shinada, *Single-atom nanoelectronics* (Jenny Stanford Publishing, 2013) p. 16.

[21] E. Prati, K. Kumagai, M. Hori, and T. Shinada, Scientific reports **6**, 19704 (2016).

[22] K. Y. Tan, K. W. Chan, M. Mottonen, A. Morello, C. Yang, J. v. Donkelaar, A. Alves, J.-M. Pirkkalainen, D. N. Jamieson, R. G. Clark, et al., Nano letters **10**, 11 (2010).

[23] M. Pierre, R. Wacquez, X. Jehl, M. Sanquer, M. Vinet, and O. Cueto, Nature nanotechnology **5**, 133 (2010).

[24] L. P. Kouwenhoven, D. Austing, and S. Tarucha, Reports on Progress in Physics **64**, 701 (2001).

[25] J. Van Donkelaar, C. Yang, A. Alves, J. McCallum, C. Hougaard, B. Johnson, F. Hudson, A. Dzurak, A. Morello, D. Spemann, et al., Journal of Physics: Condensed Matter **27**, 154204 (2015).

[26] T. I. Galkina, A. Y. Blinov, M. Bonch-Osmolovskii, O. Koblinger, K. Lassmann, and W. Eisenmenger, Physica Status Solidi B (1987).

[27] T. Klitsner and R. Pohl, Physical Review B **36**, 6551 (1987).

[28] M. Msall, M. Carroll, J. Shield, and J. Wolfe, in *Phonon Scattering in Condensed Matter VII* (Springer, 1993) pp. 116–117.

[29] G. Xie, Y. Guo, B. Li, L. Yang, K. Zhang, M. Tang, and G. Zhang, Physical Chemistry Chemical Physics **15**, 14647 (2013).